AIAA JOURNAL
Vol. 47, No. 4, April 2009

Consequences of Material Addition for a Beam Strip in a Thermal Environment

Mark A. Haney*
U.S. Air Force Research Laboratory, Wright–Patterson Air Force Base, Ohio 45433
and
Ramana V. Grandhi†
Wright State University, Dayton, Ohio 45435

DOI: 10.2514/1.41205

Aircraft structure subjected to elevated temperature presents a challenging design environment as damaging thermal stress can result. Thermal stress in a structural component is typically alleviated by accommodating the thermal expansion. However, very little work has been done that directly addresses the situation where such a prescription for expansion is not possible. When a structural component is failing due to tensile stresses which are thermally induced, the answer to the question of how best to stiffen the structure in this environment is far from trivial. This work demonstrates that conventional stiffening techniques, for example, thickness increase, may actually increase the rate of damage, as well as generate additional load that must be reacted by sub- and surrounding structure. Because flat plates represent a common structural element that is susceptible to developing tensile stresses due to thermally induced out-of-plane deformation, a simple strip model which represents cylindrical bending in a semi-infinite flat plate is chosen as the focus of this work.

Nomenclature

A	=	area cross section
$\mathbf{d}$	=	design variable vector
$\mathbf{dS}$	=	undeformed differential beam element
$\mathbf{ds}$	=	deformed differential beam element
d_i	=	components of design variable vector, $i = 1, 2$
E	=	Young's modulus
$\mathbf{F}$	=	second-order deformation gradient tensor
$\mathbf{H}$	=	tangent matrix of differential equation system
h	=	beam thickness
$\hat{h}$	=	nondimensional beam thickness
$\mathbf{I}$	=	second-order identity tensor
I	=	area moment of inertia
K_s	=	edge stiffnesses
k_s	=	spring stiffness ratio
L	=	length of beam
M	=	moment in beam
M_0	=	reaction moment at clamped edge
m	=	nondimensional reaction moment
N	=	axial internal beam force
P	=	reaction force at clamped edge
p	=	nondimensional reaction load
r	=	stretch ratio
s	=	arc length of deflected curve
$\hat{s}$	=	nondimensional arc length
u, w	=	displacement components
$\hat{u}, \hat{w}$	=	nondimensional displacements
X	=	undeformed spatial coordinate
$\mathbf{Y}$	=	boundary value problem system variable
$\tilde{\mathbf{Y}}$	=	initial value problem system variable
α	=	linear coefficient of thermal expansion
γ	=	beam geometric constant
ΔT	=	change in temperature
ε	=	axial strain
θ	=	rotation of beam cross section
κ	=	curvature of deformed beam
ξ	=	nondimensional spatial coordinate
Π	=	residual function
τ	=	nondimensional temperature

Received 24 September 2008; accepted for publication 19 November 2008.

*Research Engineer, Structural Sciences Center. Member AIAA.
†Distinguished Professor, Department of Mechanical and Materials Engineering. Fellow AIAA.

I. Introduction

SINCE the advent of high-speed flight in the mid-1950s, thermal management of critical aircraft structures has been an important design consideration. As Mach numbers rapidly increased, engineers quickly discovered that all aluminum outer skins were inadequate to meet the thermal demands with respect to maximum operating temperature. With large heat fluxes resulting from frictional and shock effects, higher temperature material systems were required. Titanium and nickel-based alloys (Inconel) replaced aluminum in most moderate temperature applications. As surface temperatures continued to increase, more exotic material systems were required to provide material thermal stability. Although maximum operating temperature is an obvious enabling concern, strain and stress magnitudes are also important to a successful thermal design.

The traditional approach to the design of thermal structures typically includes a prescription for permitting thermal expansion to take place. Thermal stresses result when this expansion is inhibited. Aerospace examples of this approach to hot structures can be found in engine liners, tailpipes, and the well-known example of the fuel system of the SR-71 [1]. This concept is not, however, unique to the aerospace industry as very familiar examples are found in expansion joints in concrete sections and in the slotted attachment of vinyl siding for home exteriors. Hence, the most efficient means of managing thermal stress is to allow expansion if that solution is available.

In addition to the heat due to aerodynamic effects, engine exhaust gases can also provide the necessary conditions for damage due to thermal stresses. The impingement of engine exhaust gases on structure was not a concern in legacy military aircraft as the engines were either situated under the wings for cargo aircraft or at the aft section for fighters. The exhaust was expelled directly into the airstream. In modern military aircraft, however, stringent requirements place greater demands on mission capability and survivability. The ability to evade enemy detection from both radar and infrared

sensors has supplanted many previously prevailing structural concerns. One location, in particular, where relief of thermal stress cannot be easily accomplished by allowing thermal expansion, is in the area of embedded engines.

Embedded engines provide the necessary low-observability characteristics to deny an enemy target which is very amenable to infrared detection. To complete the design, an engine exhaust-washed structure (EEWS) is placed aft of the engines to prevent line of sight into the engines. An EEWS, in general, consists of multiply curved shell-like skin made of a relatively high-temperature metallic which shields the low-temperature substructure from hot exhaust gases. Figure 1 provides a notional depiction of such a configuration. The shape of the EEWS is dictated by the contour (or outer mold line) of the aircraft and, to maximize thrust, the exhaust gases will be vectored to flow directly over the EEWS. Depending on the fixity of the EEWS, thermal stress and/or acoustic excitation can result. To avoid increases in signature associated with radar cross section, the EEWS must be *smoothly* integrated into the airframe. These smoothness requirements refer to the ability of the structure to attenuate incident radar waves. Gaps and junctures diminish this ability and emit spectral reflections which can be detected by radar [2].

One concept that attempts to satisfy both the smoothness requirement and accommodate thermal expansion is shown in Fig. 2. In this figure, one edge of the EEWS is shown with a knife-edge seal covering the interface. The seal is pretensioned to maintain intimate contact between the EEWS and the knife edge. The concept attempts to allow thermal expansion to take place underneath the seal. Although the seal provides a sufficiently smooth interface for a stationary (or clamped) EEWS, when motion underneath the seal is permitted, the stick-slip nature of friction can cause localized gaps to develop. Large reflections from these cavities could result, making this concept difficult to implement in a reliable manner.

The attempt to allow the hot structure to expand and contract as needed without stress resulting is often referred to as a *floating* design. The implementation of a floating design in this scenario has an additional negative consequence. If the design is allowed to float, no flight load may be reacted through the structure. This, in effect, renders the weight of the EEWS totally parasitic from a flight-loads perspective.

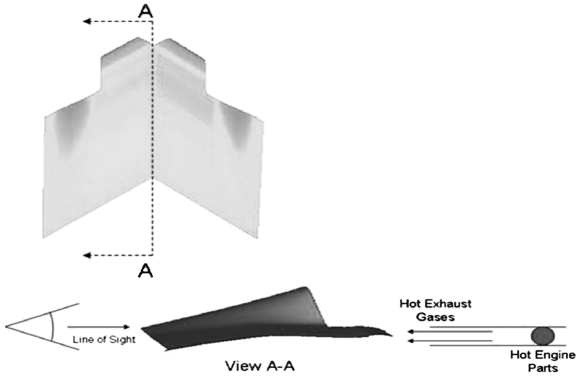

Fig. 1 Notional EEWS preventing line of sight into engine.

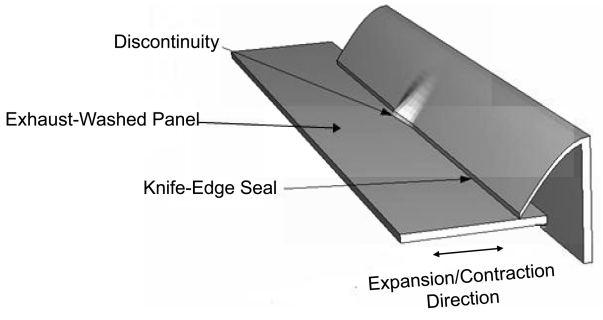

Fig. 2 Knife-edge seal attempt to allow thermal expansion of EEWS.

Because the possibility of determining a solution that relieves thermal stress while maintaining the survivability requirement seems unlikely, a decision must be made as to which requirement takes precedence. Assuming the survivability requirement is deemed more important, the EEWS must be secured to the surrounding structure and other methods developed to mitigate damaging thermal stresses which can result in cracking or failure.

With the proper motivation developed for examining a highly constrained thermal structure, this work provides several key findings as to the nonintuitive nature of material addition in a thermal environment. In Sec. II.A, we examine the case of fully constrained solutions. In Sec. II.B, we investigate the case with flexible end conditions to ensure that the general conclusions of this paper are not violated for realistic support conditions. And lastly, the conclusion section recaps the findings of this work.

II. Response and Failure Modes

Because the structure considered here can best be idealized as a shell, [3] is useful in studying the past work in thermomechanical response of plate and shell structures. Plates and shells exposed to thermal energy can respond in a variety of different ways depending on the in-plane temperature variation, through-thickness temperature gradient, and essential boundary conditions. Depending on these inputs, the panel may continuously deform out of plane (called *bowing*); however, under certain conditions, buckling and subsequent postbuckling response can occur. When studying flat plates subjected to thermal loading, buckling is the primary response and occurs at relatively low temperatures. As initial curvature is introduced into the geometry, a shell geometry results and the required buckling temperature increases [3]. This result is intuitive as buckling occurs due to instability, which forces the structure to follow bifurcated equilibrium paths. If the structure contains initial curvature, a smooth equilibrium path may exist independent of buckling which allows for thermal expansion, albeit out of plane.

The EEWS will undoubtedly be attached at many locations to the sub- and surrounding structure to prevent edge movement. Figure 3 depicts a notional cross section in which the EEWS is attached to a relatively "cold" surrounding structure. The surrounding structure provides the fixity necessary to generate out-of-plane deformation and resulting thermal stresses. If the attachment is approximated as a clamped boundary where both displacements and rotations are suppressed, the highest tensile stresses will occur on the underside of the panel, opposite the deflection. For a flat strip, this maximum tensile stress condition also exists at the center of the beam on the positive deflection side. However, for any imperfection that biases the deformation toward the out-of-plane direction, the maximum tensile stress location is unique to the ends of the beam. It should be noted that, although these locations correspond to the maximum tensile stress locations, the actual magnitude of the stresses could, in fact, be compressive due to the combination of in-plane and bending components.

A. Straight Beam Model with Clamped Edges

To determine the response characteristics of the EEWS, a simple "strip" model (beam with rectangular cross section) with idealized, clamped boundary conditions will be used to extract the essential

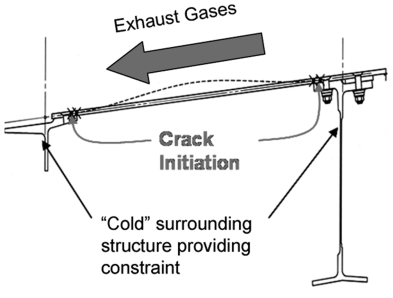

Fig. 3 Notional cross section of EEWS attachment to airframe.

features of the panel response and examine the consequences of common stiffening techniques to alleviate observed damage.

Displacement and stress response of a flat beam subjected to thermal energy input are extremely dependent on the level of fixity at the boundary. If the clamped boundary assumption is relaxed, the in-plane displacement will increase while the stress decreases. Therefore, the clamped boundary assumption provides an upper bound from both a stress perspective as well as the load that must be reacted by the surrounding structure. In the second half of this work, flexible boundary conditions are considered. To facilitate comparison with the clamped condition, the infinite stiffness condition is denoted by the purple curve on subsequent figures. We emphasize here that the general conclusions of this work are most pronounced by the clamped condition; however, similar effects are possible when the boundary stiffness is smaller.

A unit-width strip model (Fig. 4) will be used to demonstrate the nonintuitive nature of thickness increase in an elevated thermoelastic domain. The strip model permits the use of a simplified nonlinear beam theory to demonstrate the essential characteristics of cylindrical bending of a semi-infinite shell. Following an approach similar to that employed in [4–7], a planar two-point boundary value problem is solved for the postbuckling response of a clamped–clamped, thermally loaded beam by the employing the so-called shooting method for nonlinear ordinary differential equations. The focus of this work is nonlinear geometric effects which result in tensile stresses. For an initially flat beam with no imperfection, the only way tensile stresses can result is if the beam bifurcates and enters the postbuckled regime.

Figure 5 illustrates the deformed and undeformed states of an initially straight beam. The material points in the undeformed configuration are described by the pair (X, Y) with $X \in [0, L]$ and $Y = 0$. Hence, the material points, $(X, 0)$ are mapped to points $(X + u, w)$ when the beam configuration corresponds to a buckled state. An undeformed differential element **dS** is mapped into the stretched and rotated differential element **ds** in the current (or deformed) configuration. The deformations are restricted to lie in the X–Y plane and symmetry about the centerline $(X = L/2)$ is assumed. Equilibrium in the deformed configuration is shown in Fig. 6.

Symbolically, the mapping from the original to the current configuration can be expressed by

$$\mathbf{ds} = \mathbf{F}\mathbf{dS} \tag{1}$$

where **F** is the deformation tensor [8]. In terms of the displacement

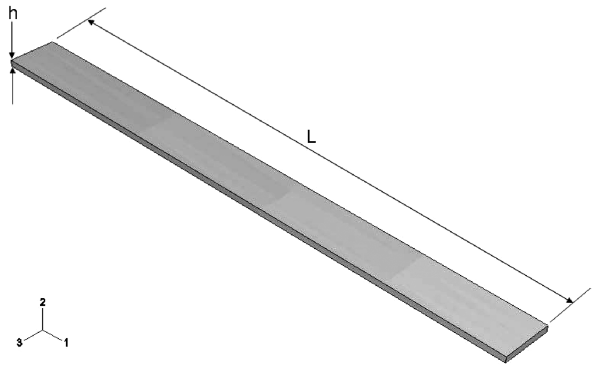

Fig. 4 Unit-width strip model.

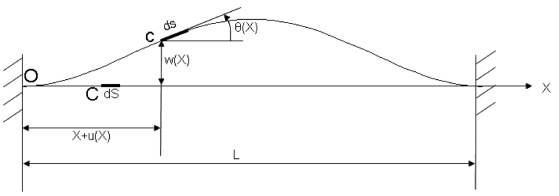

Fig. 5 Undeformed and deformed configuration of thermally loaded, clamped–clamped beam.

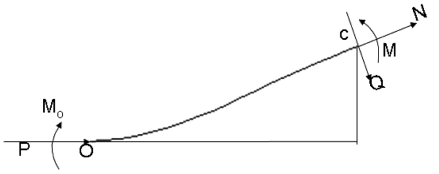

Fig. 6 Free-body diagram of deformed configuration.

gradient, **F** can be expressed as

$$\mathbf{F} = \mathbf{I} + \nabla_{\mathbf{X}}\mathbf{u}(X) \tag{2}$$

where $\nabla_{\mathbf{X}}$ represents the gradient operator with respect to the material (or Lagrangian) configuration and $\mathbf{u}(X)$ is the displacement vector. From Eqs. (1) and (2), the following geometric relations are obtained (with dependent variables suppressed):

$$\frac{|\mathbf{ds}|}{|\mathbf{dS}|} = \frac{\mathrm{d}s}{\mathrm{d}X} = r, \qquad \frac{\mathrm{d}u}{\mathrm{d}X} = r\cos\theta - 1, \qquad \frac{\mathrm{d}w}{\mathrm{d}X} = r\sin\theta$$
$$r = -\frac{P}{EA}\cos\theta + \alpha\Delta T + 1 \tag{3}$$

The strain and curvatures can be expressed in terms of r and θ by

$$\varepsilon = r - 1, \qquad \kappa = \frac{1}{r}\frac{\mathrm{d}\theta}{\mathrm{d}X} \tag{4}$$

The thermoelastic constitutive equations are given by

$$N = EA(\varepsilon - \alpha\Delta T), \qquad M = EI\kappa \tag{5}$$

If forces and moments are summed at the left-hand end of Fig. 6 (point "O"), the resulting equilibrium equations are given by

$$N + P\cos\theta = 0, \qquad M + Pw = M_o \tag{6}$$

where $s(X)$ is the arc length of the deflected curve, $r(X)$ is the stretch ratio of the axial line, $\theta(X)$ is the cross-sectional rotation, $N(X)$ is the axial internal force, and $M(X)$ is the internal bending moment. P is the constraint reaction force at the clamped boundary, M_o is the reaction moment at the constrained ends, E is the Young's modulus, α is the linear thermal expansion coefficient, A is the cross-sectional area, I is the second moment of area of the cross section, and ΔT is the change in temperature of the uniform field. For this study, no temperature dependence is assumed for the properties; however, because a uniform temperature field is assumed throughout the beam, the "at-temperature" properties will be used.

For solution convenience, the following dimensionless variables will be used:

$$(\xi, \hat{s}, \hat{u}, \hat{w}, \hat{h}) = \frac{1}{L}(X, s, u, w, h), \qquad \tau = \gamma^2\alpha\Delta T \qquad \gamma = L\sqrt{\frac{A}{I}}$$
$$p = \frac{PL^2}{EI}, \qquad m = \frac{M_o L}{EI} \tag{7}$$

The nonlinear system of dimensionless equations are given by

$$\hat{s}'(\xi) = r, \qquad \hat{u}'(\xi) = r\cos\theta - 1 \qquad \hat{w}'(\xi) = r\sin\theta$$
$$\hat{\theta}'(\xi) = r(m - p\hat{w}) \qquad p'(\xi) = m'(\xi) = 0 \tag{8}$$

where r, in terms of nondimensional variables, is given by $r = (-p\cos\theta + \tau)/\gamma^2 + 1$. The symmetric boundary conditions for the nonlinear system are

$$\hat{s}(0) = \hat{u}(0) = \hat{w}(0) = \theta(0) = 0 \qquad \hat{u}(\tfrac{1}{2}) = \theta(\tfrac{1}{2}) = 0 \tag{9}$$

The dimensionless temperature τ is treated as a prescribed parameter in the solution process. Physically, this makes sense, as the dimensional temperature is a prescribed value in the original form of the equations. For values of τ greater than $4\pi^2$, buckling occurs [6].

To compute the large displacement, out-of-plane deformation, a shooting method for solving nonlinear ordinary differential equations is used to solve the system of equations. Symbolically, the system can be expressed as [7]

$$\frac{\mathrm{d}\mathbf{Y}(\xi)}{\mathrm{d}\xi} = \mathbf{H}(\xi, \mathbf{Y}(\xi); \tau) \qquad (0 \le \xi \le \tfrac{1}{2})$$
$$\mathbf{B}_1\mathbf{Y}(0) = \{\,0 \quad 0 \quad 0 \quad 0\,\}^T, \qquad \mathbf{B}_2\mathbf{Y}(0) = \{\,0 \quad 0\,\}^T$$
$$\mathbf{Y} = \{\,y_1 \quad y_2 \quad y_3 \quad y_4 \quad y_5 \quad y_6\,\}^T = \{\,\hat{s} \quad \hat{u} \quad \hat{w} \quad \theta \quad m \quad p\,\}^T$$
$$\mathbf{H} = \{\,r \quad r\cos y_4 - 1 \quad r\sin y_4 \quad r(y_5 - y_3 y_6) \quad 0 \quad 0\,\}^T$$
$$\mathbf{B}_1 = \begin{bmatrix} 1 & 0 & 0 & 0 & 0 & 0 \\ 0 & 1 & 0 & 0 & 0 & 0 \\ 0 & 0 & 1 & 0 & 0 & 0 \\ 0 & 0 & 0 & 1 & 0 & 0 \end{bmatrix}, \qquad \mathbf{B}_2 = \begin{bmatrix} 0 & 1 & 0 & 0 & 0 & 0 \\ 0 & 0 & 0 & 1 & 0 & 0 \end{bmatrix} \tag{10}$$

In actuality, m and p are problem parameters. These load terms are treated as unknown functions of ξ (even though they are single point values at $\xi = 0$) forming a standard problem statement for accommodating nonlinear boundary value problems with multiple parameters [9].

The shooting method for the solution of nonlinear ordinary differential equations involves reformulating the problem in terms of an initial value problem:

$$\frac{\mathrm{d}\tilde{\mathbf{Y}}(\xi)}{\mathrm{d}\xi} = \mathbf{H}(\xi, \tilde{\mathbf{Y}}(\xi); \tau) \qquad (0 \le \xi \le \tfrac{1}{2})$$
$$\tilde{\mathbf{Y}}(0) = \{\,0 \quad 0 \quad 0 \quad 0 \quad m(0) \quad p(0)\,\}^T \tag{11}$$

The initial value problem is iteratively solved using an appropriate integrator (i.e., fourth-order Runge–Kutta) until the conditions at $\xi = \frac{1}{2}$ match the prescribed values. This problem can be treated as an optimization problem with the objective being satisfaction of the end conditions, whereas the unprescribed values at $\xi = 0$, $m(0)$; $p(0)$ are treated as design variables. If we define the design variable vector $\mathbf{d} = \{\,y_5(0) \quad y_6(0)\,\}^T$, then the current estimate of the initial value problem can be treated as a function of the design variables,

$$\frac{\mathrm{d}\tilde{\mathbf{Y}}(\xi, \mathbf{d})}{\mathrm{d}\xi} = \mathbf{H}(\xi, \tilde{\mathbf{Y}}(\xi, \mathbf{d}); \tau) \qquad \left(0 \le \xi \le \tfrac{1}{2}\right)$$
$$\tilde{\mathbf{Y}}(\mathbf{0}) = \{\,0 \quad 0 \quad 0 \quad 0 \quad d_1 \quad d_2\,\}^T \tag{12}$$

The primal problem [Eq. (12)] can be differentiated to compute analytical sensitivities of the response with respect to the design variables. This direct differentiation method [10] is given by the two following pseudoproblems:

$$\left(\frac{\mathrm{d}\tilde{\mathbf{Y}}(\xi, \mathbf{d})}{\mathrm{d}\xi}\right)_{,d_1} = \mathbf{H}_{,\tilde{\mathbf{Y}}}(\xi, \tilde{\mathbf{Y}}(\xi, \mathbf{d}); \tau)\tilde{\mathbf{Y}}_{,d_1} \qquad \left(0 \le \xi \le \tfrac{1}{2}\right)$$
$$\tilde{\mathbf{Y}}_{,d_1}(\mathbf{0}) = \{\,0 \quad 0 \quad 0 \quad 0 \quad 1 \quad 0\,\}^T$$
$$\left(\frac{\mathrm{d}\tilde{\mathbf{Y}}(\xi, \mathbf{d})}{\mathrm{d}\xi}\right)_{,d_2} = \mathbf{H}_{,\tilde{\mathbf{Y}}}(\xi, \tilde{\mathbf{Y}}(\xi, \mathbf{d}); \tau)\tilde{\mathbf{Y}}_{,d_2} \qquad \left(0 \le \xi \le \tfrac{1}{2}\right) \tag{13}$$
$$\tilde{\mathbf{Y}}_{,d_2}(\mathbf{0}) = \{\,0 \quad 0 \quad 0 \quad 0 \quad 0 \quad 1\,\}^T$$

The residual system of equations to be solved is expressed by

$$\Pi(\mathbf{d}^*) = (\tilde{\mathbf{Y}}(\xi, \mathbf{d}^*) - \mathbf{B}_2\mathbf{Y}(\xi))_{\xi=\frac{1}{2}} = \mathbf{0} \tag{14}$$

Where $\mathbf{d}^*$ denotes the optimal value of $\mathbf{d}$. Expanding Eq. (14) in a first-order Taylor series expansion gives

$$\Pi(\mathbf{d}^*) = \Pi(\mathbf{d}^i) + \left(\frac{\partial\Pi(\mathbf{d})}{\partial\mathbf{d}}\right)_{\mathbf{d}=\mathbf{d}^i}\Delta\mathbf{d}^i \approx \mathbf{0} \tag{15}$$

Solving Eq. (15) for $\Delta\mathbf{d}^i$,

$$\Delta\mathbf{d}^i \approx -\left(\frac{\partial\Pi(\mathbf{d})}{\partial\mathbf{d}}\right)^{-1}_{\mathbf{d}=\mathbf{d}^i}\Pi(\mathbf{d}^i) \tag{16}$$

The update for the design variables becomes

$$\mathbf{d}^{\,i+1} = \mathbf{d}^i + \Delta\mathbf{d}^i \tag{17}$$

Equations (15–17) facilitate the application of Newton's method for the solution of the nonlinear system with $\mathbf{d}^i$ the current estimate of the design variables.

Thermally buckled configurations are shown in Fig. 7 for various values of nondimensional temperature τ. For a clamped–clamped isotropic strip, one location of maximum tensile stress occurs at the clamped edge at the outermost fibers opposite the displacement. Hence, for the case under consideration, the maximum tensile stress occurs at point "O" (see Fig. 5) on the bottom of the strip. If the strip is perfectly flat (without imperfection), the same maximum stress is realized at the center of the strip for the clamped condition. However, with stress concentrations induced due to fastening methods, the ends of the strip constitute the most likely damage location.

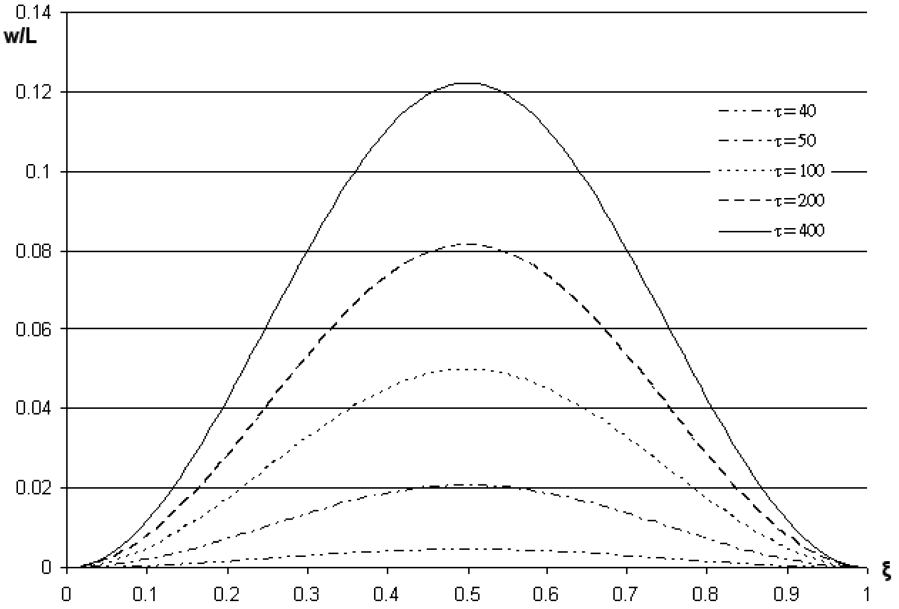

Fig. 7 Postbuckled configurations for various values of nondimensional temperature.

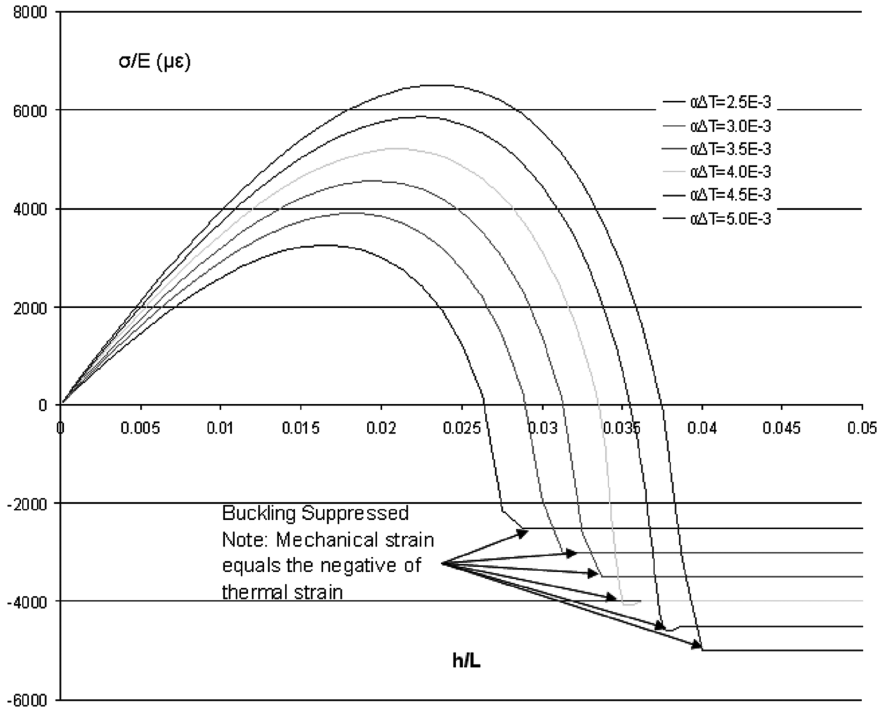

Fig. 8 Maximum mechanical strain vs normalized thickness for various values of thermal strain.

One of the most common approaches to alleviating thermal buckling is to increase the thickness of the panel. The minimal value of τ for which buckling occurs is computed by the solution of the linearized eigenvalue problem in Eq. (10). The critical value of τ at which buckling occurs is $4\pi^2$. From Eq. (7), with $\tau = 4\pi^2 = \gamma^2\alpha(\Delta T)_{\text{cr}}$, a decrease in γ increases the temperature change required to initiate buckling. The nondimensional thickness is related to γ^2 by

$$\gamma^2 = L^2\frac{A}{I} = L^2\left(\frac{h}{1/12h^3}\right) = \frac{12}{(h/L)^2} = \frac{12}{\hat{h}^2} \tag{18}$$

Therefore, a factor of 2 increase in thickness increases the critical buckling temperature by a factor of 4. Although this *is* an efficient means to increase buckling temperature, the increased load due to participation of the additional thermal mass must be reacted by the surrounding structure. Therefore, care must be taken to ensure the structural integrity of the sub- and surrounding structure. Additionally, if an attempt is made to prohibit buckling and, due to model uncertainty (e.g., boundary conditions, material properties, etc.), the desired buckling temperature is underpredicted, an *increase* in tensile stress can be observed in the skin.

Figure 8 presents the results of a study examining the influence of strip thickness on maximum *mechanical* strain. Note the parabolic behavior of the strain response at the beam edge with thickness. For a given material and temperature change, there exists a maximum strain condition corresponding to a particular value of nondimensional thickness. This result differs dramatically from typical mechanically loaded cases where increases in thickness decrease the stress monotonically. In fact, if geometric nonlinearity is ignored, a monotonic decrease in stress is also observed in the thermoelastic beam problem for realistic values of thickness [11]. The value of strain and normalized thickness for the case $\alpha\Delta T = 0.005$ are given in Table 1.

Figure 8 demonstrates that increasing thickness does not necessarily lower the edge stresses and can, in many circumstances, increase the stress levels. Another important consideration is the additional load that is transferred to the fixed boundary. The fixed boundary assumption provides an upper bound on the potential load that can be generated. From Fig. 9, with $\alpha\Delta T = 0.005$, the increase in load P is proportional to the nondimensional load p and the cube of the nondimensional thickness $\hat{h}^3$:

$$P \sim p(\tilde{h})\tilde{h}^3 \tag{19}$$

The nondimensional load $p(\tilde{h})$ is very nearly constant over the range of $\tilde{h}$ up to the point where buckling is indeed suppressed (Fig. 9). Hence, in this region, $\tilde{h}^3$ dominates the relation. At thicknesses at which buckling is suppressed and greater, a constant linear increase in reaction load at the boundary is observed. Because the load for an unbuckled, unit-width, flat, rectangular beam is given by $P = (E\alpha\Delta T)h$, these results are consistent.

The slope of the load curve is greatest just below the buckling suppression point. Therefore, if an attempt is made to suppress buckling by increasing thickness and this point is missed due to model inadequacy, a large increase in load is observed for even small increases in thickness. This behavior is similar to what was observed in the strain-vs-thickness behavior. The primary conclusion to be drawn from this exercise is that an increase in thickness results in a monotonic increase in load to the boundary, which, in a realistic structure, will be reacted by the sub- and surrounding structure to which it is attached. So material, being used to stiffen a structure in a thermal environment, should be used sparingly and judiciously to accomplish the two objectives of minimal boundary load increase and stress reduction.

B. Straight Beam Model with Elastic End Conditions

In the previous section, fixed-end conditions were exclusively considered. In this section, the influence of flexibility at the boundary will be addressed. With flexible end conditions, the possibility exists that the results of the previous section could be called into question. However, one indication that the conclusions reached in the

Table 1 Mechanical strain vs h/L for thermal clamped–clamped beam with $\alpha\Delta T = 0.005$

h/L	Microstrain
0.0001	44.1
0.0051	2143
0.010	3970
0.020	6301
0.040	−5000

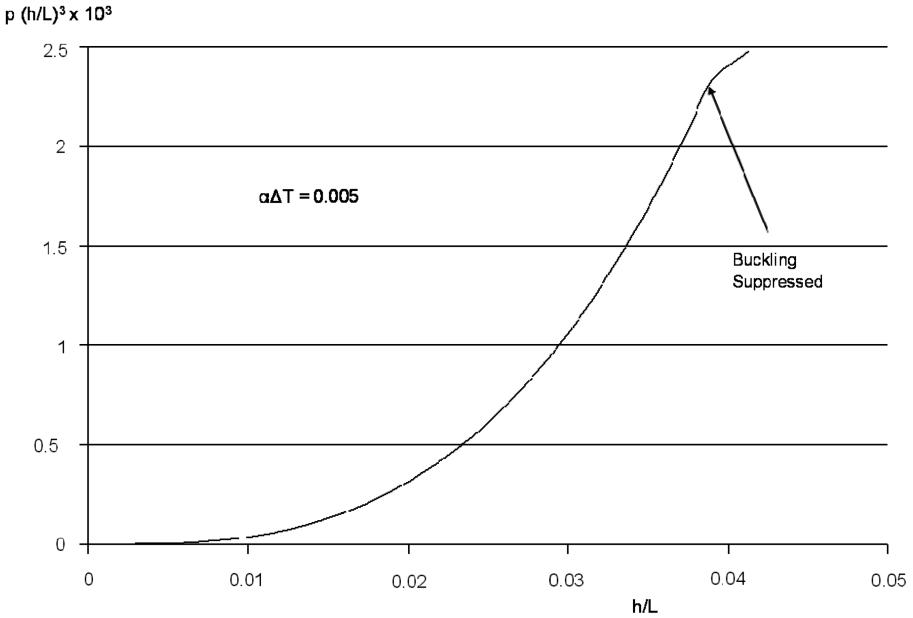

Fig. 9 Effect of increasing thickness on nondimensional reaction force for clamped–clamped beam.

fixed-end case will remain valid is given in Fig. 10. This curve was taken from [12] and represents the results of a buckling study of flat, simply supported plates with edge spring supports to constrain the in-plane displacements. Note that, at large values of relative spring stiffness, the curve is rather flat. This implies that decreases in relative spring stiffness between the panel and the boundary have little effect on the buckling temperature when the boundary stiffnesses are large. Therefore, as the stiffness of the panel is increased (e.g., increasing thickness) relative to the boundary stiffness, the initial indication is that stresses may not be reduced until a given ratio of stiffness is obtained. This phenomenon is investigated in this section.

Because the damage location of interest is coincident with the boundary, edge rotations will again be suppressed, however, finite edge displacements will be permitted as thermal expansion takes place. Figure 11 illustrates the geometry in linear springs are placed at $X = 0$ and $X = L$. This choice of placement maintains symmetry in the problem formulation. In [6], Li et al. introduce a spring at $X = 0$ but maintain a simple-supported boundary at $X = L$ which destroys symmetry in the undeformed configuration. However, they overcome this difficulty by expressing the deformation gradient derivatives with respect to deformed variables.

The commercial nonlinear finite element code ABAQUS is used to conduct a parametric study of the influence of the edge spring stiffness. A linear thermal buckling analysis is initially performed. The first buckled shape is then used to seed the subsequent nonlinear analysis with a small imperfection. Because the thickness is changed in each analysis run, the initial imperfection is scaled to 5% of the current thickness for each analysis performed. A study was performed to insure that the results were independent of the perturbation size and that they did not influence the desired responses. A temperature of 900°F was applied to the strip with a thermal expansion coefficient of 5×10^{-6}°F. A constant, at-temperature value of Young's modulus of 10^7 psi was used. These material properties coincide closely with certain titanium alloys. A mesh convergence study was conducted and a mesh size of 0.1 in. over the 12 in. beam length was found adequate to predict the buckling temperature difference. Because the potential exists for large out-of-plane displacement, nonlinear geometric effects were included in all analyses.

Along with the nondimensional quantities used in the previous section, an additional variable is introduced which represents the relative stiffness of the strip to that of the boundary spring K_s:

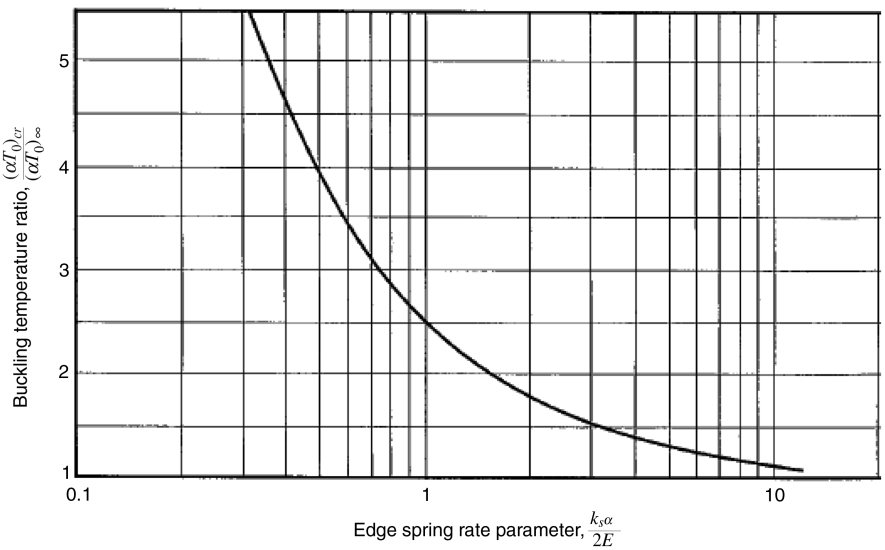

Fig. 10 Spring stiffness vs buckling temperature ratio [12].

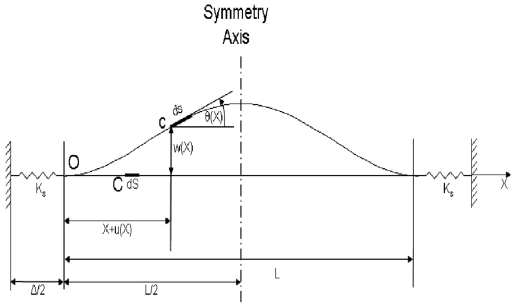

Fig. 11 Undeformed and deformed configuration of thermally loaded beam with spring supports.

$$k_s = \frac{K_s}{EA/L} \tag{20}$$

Although this ratio differs from the nondimensionalization necessary for problem-independent solutions [6], scaling by the familiar beam stiffness EA/L provides greater insight for physical systems. Figure 12 details the influence on critical buckling temperature ratio as the thickness of the panel is increased. The y axis in this figure is the ratio of the current value of ΔT necessary to buckle the panel of thickness h to the value of ΔT with fixed boundary conditions and a thickness of h_o.

Figure 12 is especially useful in evaluating a possible repair scenario in which the repair consists of adding material to the thickness of the failing panel. If we examine Fig. 12 at a thickness ratio of 2 (which corresponds to doubling the thickness), the buckling temperature increases by a factor of 4 for the infinite edge stiffness condition. When considering a finite stiffness ratio, the reader should be aware that the finite stiffness curves are, in fact, a function of the thickness. So, for example, if the failing design corresponds to an initial stiffness curve of 10, a doubling of the thickness would halve the relative stiffness ratio, placing the new relative stiffness at a value of 5. Referring again to Fig. 12, at a thickness ratio of 2 for the relative stiffness value 5 gives an approximate critical buckling ratio increase of 7.5. Therefore, if the operating temperature is greater than a factor of 7.5 above the original buckling temperature, the panel could continue to buckle. Hence, as was shown in the fixed edge case, the possibility exists that the postbuckled state of the thicker panel could produce higher tensile stresses than were observed in the postbuckled state of the thinner, failing panel.

Another important observation that can be gleaned from the preceding results is, as the initial boundary stiffness decreases (i.e., weaker springs), adding thickness to the panel has an ever-increasing influence on the magnitude of buckling temperature. This fact is reflected in the average slope of each curve. As k_s decreases, the slope increases. If the original boundary stiffness were nonexistent (free-edge), then the buckling temperature, as well as the slope of the $k_s = 0$ curve, would approach infinity. Small values of k_s are of little interest due to the fact that failures of the original structure (thickness h) would be unlikely. Because the quantitative behavior varies widely with boundary stiffness, a premium is placed on the accuracy to which the boundary stiffness is determined. For example, if the boundary stiffness is underestimated in the model, adding thickness could appear to be a very feasible solution from a stress reduction viewpoint along with only minimal increases in additional load into surrounding structure. In fact, if a repair is necessary, the root cause could be attributed to inaccurate design values of boundary stiffness. For the repairer to take advantage of the larger increases in buckling temperature for finite values of boundary stiffness, the boundary stiffness values should be determined experimentally. However, this is not a trivial matter, as validation instrumentation is not reliable at high temperature.

As was discussed in the previous section concerning the fully clamped case, the additional load transferred into the boundary must also be considered for the flexible case. Both the increase in reaction force and moment are of concern, as these additional loads will be reacted by the sub- and surrounding structure. Furthermore, the surrounding structure may have little or no margin for carrying this additional load if the thickness increase is part of a repair. Figures 13 and 14 provide an illustration of the reaction force and moment increases, respectively, for associated increases in thickness. Examining Fig. 13, we see that, for small values of boundary stiffness, only small increases in reaction forces are possible. For large values of initial boundary stiffness ratio, the loads increase very rapidly with the infinite stiffness condition providing an upper bound. Note that, up to approximately 2 times the original thickness, the stiffness ratios of 5 and 10 are both approximated well by the fixed condition. As the thickness continues to increase, the infinite stiffness condition provides an upper bound and can be used as a conservative design point.

Another important bound can be deduced if we examine the spring stiffness of the boundary and imagine the skin expanding freely. This free, in-plane expansion, multiplied by the boundary spring stiffness provides an upper bound on the reaction force produced. Although this load is not theoretically possible because the skin is not free to expand unabated, it does provide a useful metric for comparison if the boundary stiffness ratio is known to a high-degree of certainty. This condition corresponds to the situation in which the stiffness of the beam is much greater than that of the boundary. This can occur if the thickness is increased by several multiples.

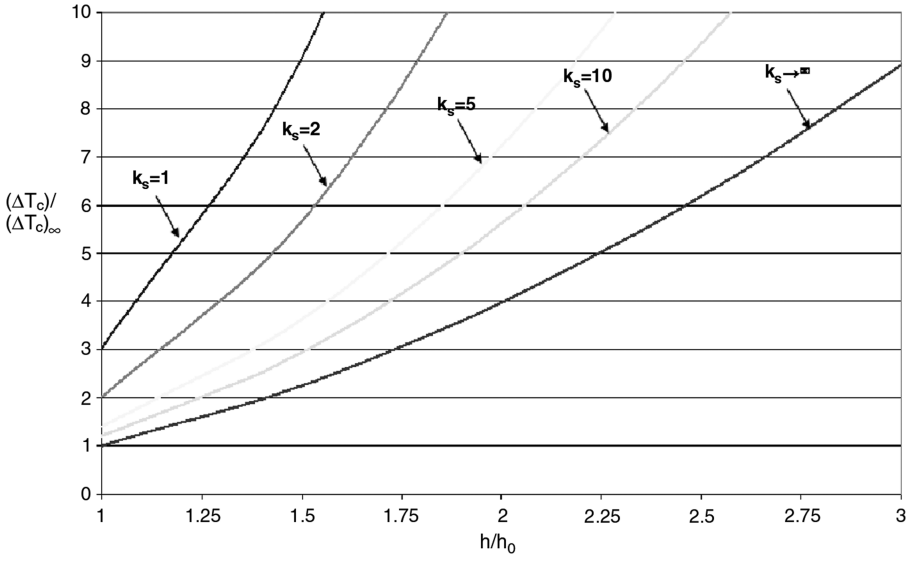

Fig. 12 Buckling temperature ratio vs h/h_0 for various values of end spring stiffnesses.

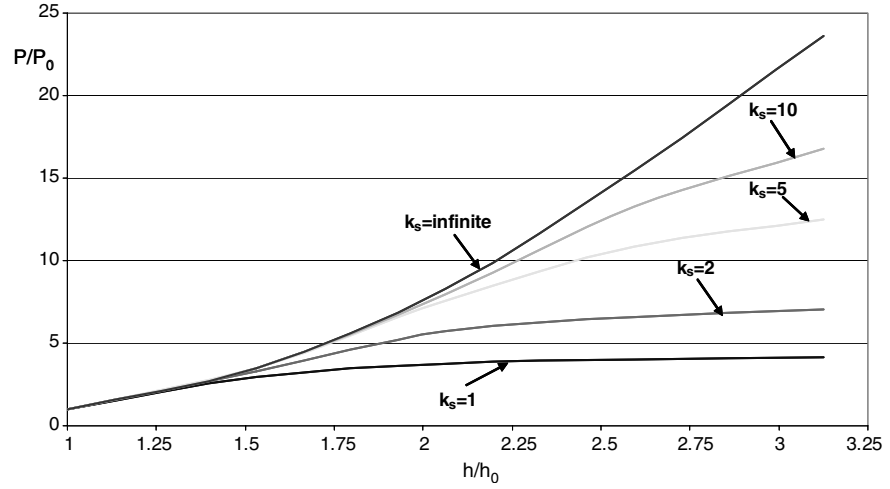

Fig. 13 Reaction force increase vs thickness increase for various stiffness ratios.

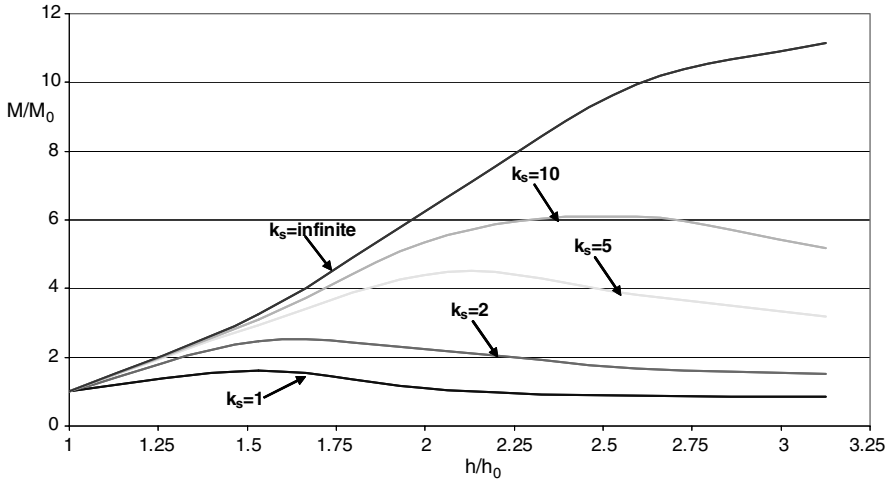

Fig. 14 Moment increase vs thickness increase for various stiffness ratios.

The moment curve in Fig. 14 demonstrates similar behavior to that found in the previous clamped beam study. The moment initially increases with increasing thickness, reaches a maximum, and then tails off as out-of-plane deformation is eventually suppressed due to the buckling temperature exceeding the operational temperature. Again, we notice that, as the boundary stiffness is reduced, less potential exists for generating large moments. As in the reaction force, the infinite stiffness case provides an upper bound on possible moment increases. The stiffness ratio of 10 is sufficiently approximated by the fixed case up to thickness ratios of 2. Note that, because an initial imperfection is seeded into the geometry, the zero moment condition (perfectly flat beam) does not exist.

Although the additional loads into the surrounding structure are of the utmost importance, the stress response also reveals the importance of knowledge about the stiffness of the boundary. Axial stresses generated by the combination of in-plane load and bending moment are shown in Fig. 15. This graph is very revealing in that it demonstrates that, although the goal of adding material was to decrease the stress in the panel, in fact, the stresses can increase for large values of boundary stiffness when material is added uniformly as a thickness increase. If we examine closely the $k_s = 10$ curve at double the original thickness, although we have dramatically increased the loads into the boundary, the stress is virtually the same as the unstiffened panel.

In the case of a crack repair, if a doubler (another strip identical to the original) is attached over the crack on the high stress side opposite the deformation, the outermost fibers of the new double thickness stackup would replace the single-thickness skin as the location of highest stress. Although this action would retard additional damage of the original panel being near the neutral axis of the two strip combination, new cracking would appear in the doubler. Therefore, this approach would provide a temporary fix and would require routine inspection and replacement of the doubler. If, however, the crack has grown completely through the panel and the repair consists of placing the doubler on the side opposite the maximum stress location, the cracking may continue at the same rate or even increase.

This study confirms the findings in the clamped case investigation and further demonstrates that the addition of material in a thermal environment that is intended to alleviate damage must be approached with extreme caution and with careful consideration given to the trade space of additional load and stress reduction.

III. Conclusions

In this paper, the very common practice of increasing thickness to suppress damage due to out-of-plane deformation of flat panels is challenged. When adding material in a thermal environment to arrest damage due to bending stresses, the contribution of the additional material to the response must be considered. Additional loads will be generated at the boundaries from this approach. Boundary stiffness plays a major role in determining the magnitude of load increase for the scenarios presented in this work. Although thickness increase was the parameter being studied here, these results also provide a general conceptual basis for examining other structural members that are employed to accomplish similar goals. For example, the effectiveness of adding I or T beams to prevent bending in a thermal environment must also be examined in this light as they too result in additional boundary load.

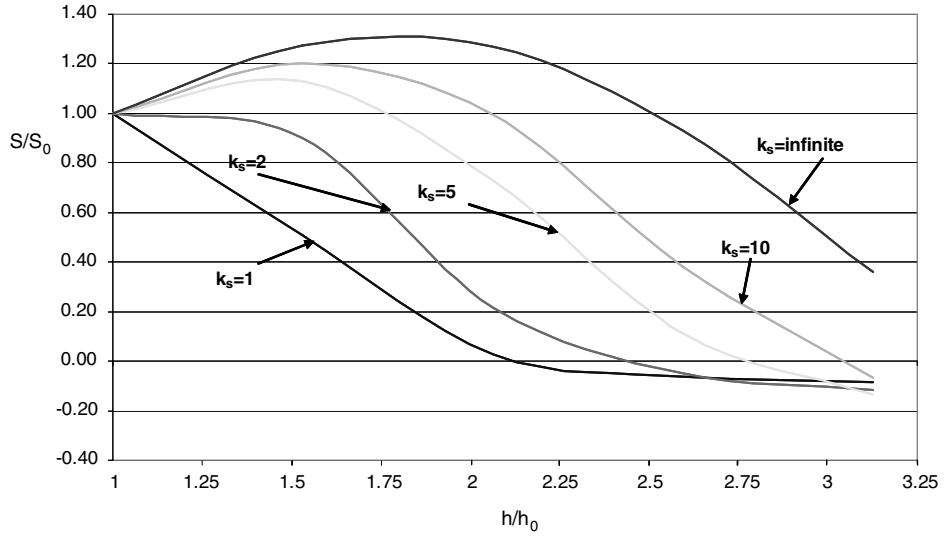

Fig. 15 Stress ratios vs thickness ratio for various values of spring stiffness ratio.

In future work, topology optimization techniques will be used to determine the optimal stiffener configuration that balances the additional load into the surrounding structure with out-of-plane deformation reduction for a flat beam with an initial imperfection. It is anticipated that the optimization will produce multiply connected regions which allow internal expansion to relieve thermal expansion forces. In fact, recent work at NASA [13] reveals that certain rectangular plates with holes actually have a higher buckling temperature than the geometry absent the hole.

Acknowledgment

The authors would like to acknowledge the U.S. Air Force Research Laboratory for supporting this research effort.

References

[1] Thornton, E. A., *Aerospace Thermal Structures and Materials for a New Era*, AIAA, Washington, D.C., 1995.

[2] Knott, E. F., Shaeffer, J. F., and Tuley, M. T., *Radar Cross Section*, 2nd ed., SciTech Publishing, New York, 2005.

[3] Thornton, E. A., "Thermal Buckling of Plates and Shells," *Applied Mechanics Reviews*, Vol. 46, No. 10, Oct. 1993, pp. 485–506.

[4] Li, S., and Cheng, C., "Analysis of Thermal Post-Buckling of Heated Elastic Rods," *Journal of Applied Mathematics and Mechanics*, Vol. 21, No. 2, 2000, pp. 133–140. doi:10.1007/BF02458513

[5] Vaz, M. A., and Solano, R. F., "Thermal Postbuckling of Slender Elastic Rods with Hinged Ends Constrained by a Linear Spring," *Journal of Thermal Stresses*, Vol. 27, No. 4, 2004, pp. 367–380. doi:10.1080/01495730490427591

[6] Li, S., Zhou, Y-H, and Zhenq, X., "Thermal Post-Buckling of a Heated Elastic Rod with Pinned-Fixed Ends," *Journal of Thermal Stresses*, Vol. 25, No. 1, 2002, pp. 45–56. doi:10.1080/014957302753305862

[7] Vaz, M. A., and Solano, R. F., "Postbuckling Analysis of Slender Elastic Rods Subjected to Uniform Thermal Loads," *Journal of Thermal Stresses*, Vol. 26, No. 9, 2003, pp. 847–860. doi:10.1080/01495730306293

[8] Gurtin, M. E., *An Introduction to Continuum Mechanics*, Academic Press, New York, 1981.

[9] Press, W. H., Flannery, B. P., and Teukolsky, S. A., *Numerical Recipes: The Art of Scientific Computing*, Cambridge Univ. Press, New York, 1989.

[10] Haftka, R. T., and Gurdal, Z., *Elements of Structural Optimization*, 3rd ed., Kluwer Academic, Dordrecht, The Netherlands, 1991.

[11] Young, W. C., *Roark's Formulas for Stress and Strain*, 6th ed., McGraw–Hill, New York, 1989.

[12] Wilcox, M. W., and Clemmer, L. E., "Large Deflection Analysis of Heated Plates," *Journal of the Engineering Mechanics Division, Proceedings of the American Society of Civil Engineers*, Vol. 90, No. 6, 1964, pp. 165–189.

[13] Ko, W. L., "Mechanical and Thermal Buckling Behavior of Rectangular Plates with Different Central Cutouts," NASA TM-1998-206542, March 1998.

E. Livne
Associate Editor